German Aerospace Center (DLR)

Internal Report 515-05-04

Real-Time Models for Wheels and Tyres

Dirk Zimmer

July 5, 2005

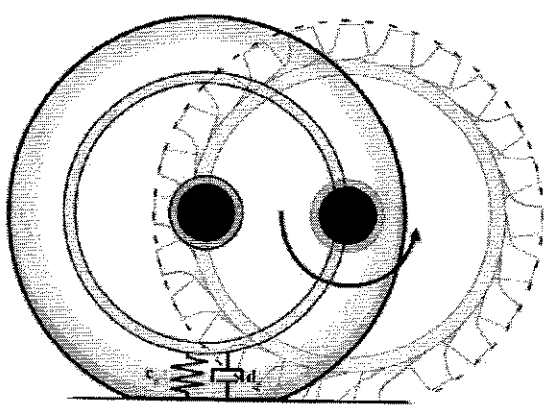

Institute of Robotics and Mechatronics
Oberpfaffenhofen

DLR

Contents

Acknowledgements

This work wouldn't have been possible without the great support of Prof. Martin Otter and Dr. Johan Bals. I'd like to thank as well Prof. Karl J.Aström who initiated this work and Prof. François E. Cellier who did the arrangement and introduced me to the Modelica language and the work with Dymola. Off course I am indebted to my family and friends for all their patience and support.

Chapter 1

Introduction

Models of wheels and tyres exist at all levels of complexity. The variability of approaches ranges from purely empirical models with the aid of regression techniques to complex models of the theoretical physical behavior.

The approach taken in this report is to start with the most simple physical model and to introduce further complexity step by step. Hence, seven models of wheels and tyres are presented. Each model at a new level of complexity.

The first simple models for ideal rolling or rigid wheels are enhanced to more elaborated versions for wheels with tyres. The lateral and longitudinal deformation of the tyre has been taken into account for the most complex models. A wheel's behavior is also strongly influenced by its shape and therefore three different wheel shapes are supported by all models.

The following targets were kept in mind at all stages of development:

- The wheel should not be restricted to certain driving situations. The model is thought to work in all relevant cases.
- The model should be as general as possible without loosing to much accuracy. It should be a usable starting point for bicycle wheels as well as for truck wheels.
- A real-time simulation of the model should be possible.
- The characteristics of the tyre should be describable with a minimum effort.

A Modelica Library "WheelDynamics" has been developed according to the models presented in this report. It builds up on the MultiBody[4] Library in the standard Modelica Package.

1.1 Structure

After the discussion of the basic geometry in chapter 2 the actual physical equations for each level of model complexity are presented in the chapters 3 to 8, where each chapter represents one level of complexity and chapter 7 summarizes the levels 5 and 6. Last but not least a solution for uneven terrain is presented in chapter 9.

The understanding of all previous chapters is a prerequisite for each new chapter. Most of the variables are only introduced once and the single models build up on each other. It is therefore strongly recommended to follow the order of this text.

1.2 Notations

All symbols that represent vectors or matrices are printed in bold face. The appendage $_{,0}$ denotes that the vector is resolved in the inertial frame. Unit vectors are denoted by an **e** and are always resolved in the inertial frame. An overview over all symbols can be found in the appendix.

1.3 References

Most of chapter 6 and 7 recapitulate major parts of a tyre model presented by Georg Rill[1]. The modified computation of the camber slip was inspired by a sketch in the book of Pacejka[2]. The adaption to a freely moving body, the improvements for low rolling velocities(the idea not to compute the slip) and the modification for the turning friction computation are contributions of this report. The contact point is computed more precisely and therefore the implementation of an explicit tilt momentum has become redundant.

This report is the result of a internship at the Research Center DLR (Deutsches Zentrum für Luft und Raumfahrt) in the Institute of Robotic and Mechatronics at the Department of Control Design Engineering. The internship started at the first of April 2005 and its durations was 3 months and a week.

Chapter 2

Geometry

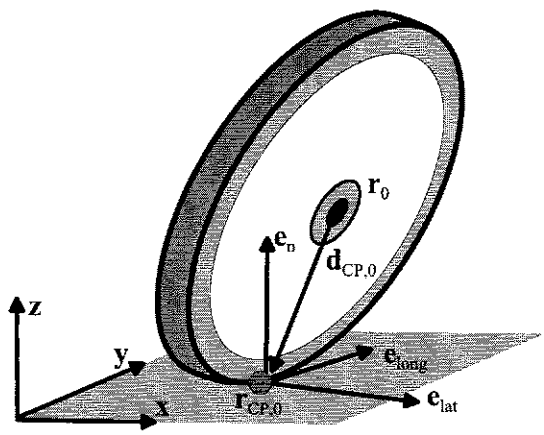

Figure 2.1: A wheel in contact with the (blue) xy-plane. All vectors in this figure are resolved in the inertial frame.

2.1 Road

It is made the overall assumption that the road is an even plane. This plane is given by a normal vector $\mathbf{n}$ and its normalized variant $\mathbf{e}_n$ and by the distance d of the plane to the origin. It's therefore defined by:

$$\mathbf{e}_n \cdot \mathbf{x} = d \tag{2.1}$$

When the wheel is on the road, we are interested in the point of contact: $\mathbf{r}_{CP,0}$. The computation of the contact point might wildly differ in dependence on the wheel geometry, but it can often easily computed for convex shapes. In the next section the computation of the contact point for different wheel shapes is presented. The geometry of the wheel won't matter thenceforward since $\mathbf{r}_{CP,0}$ is

assumed to be given for all considerations going beyond this chapter. An extension to handle uneven surfaces is sketched in chapter 9.

2.2 Wheel shapes

Three different shapes are presented: A flat disc, a torus and a voluminous wheel. To compute the contact point, two additional vectors are introduced: $d_{CP,0}$ and $e_{wheelAxis}$. $e_{wheelAxis}$ is a unit vector pointing in direction of the wheel axis and $d_{CP,0}$ points from the wheel center to the contact point:

$$\mathbf{r}_{CP,0} = \mathbf{r}_0 + \mathbf{d}_{CP,0} \tag{2.2}$$

Both vectors are resolved in the inertial frame.

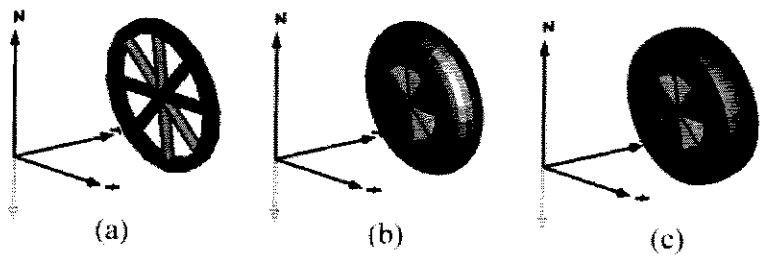

Figure 2.2: Three different wheel shapes: (a) flat disc, (b) torus (c) vol. wheel

2.2.1 Flat disc

The wheel is modelled as a flat disc with a given radius and width zero. Therefore the contact point is always located on the wheel plane and $d_{CP,0}$ is perpendicular to the wheel axis. $d_{CP,0}$ is the projection of $-e_n$ on the wheel plane with length r:

$$\mathbf{d}_{CP,0} = r \cdot normalize(\mathbf{e}_n - (\mathbf{e}_n \cdot \mathbf{e}_{wheelAxis})\mathbf{e}_{wheelAxis}) \tag{2.3}$$

where

$$normalize(\mathbf{x}) = \frac{\mathbf{x}}{|\mathbf{x}|} \tag{2.4}$$

2.2.2 Torus

A torus with outer radius r and a certain width is used to describe the geometry of the wheel. The torus is just as well defined by two radii: The inner radius $r_i = r - (width/2)$ and the torus radius

$r_t = width/2$. $\mathbf{d}_{CP,0}$ can be considered as summation of two vectors d_1 and d_2. d_2 points from the inner circle (with radius r_i) to the contact point with length r_t and is always parallel to $\mathbf{e}_n$. d_1 points from the wheel center to the outer circle and is again found by the projection of $-\mathbf{e}_n$ on the inner circle plane. Therefore:

$$\mathbf{d}_{CP,0} = \underbrace{\left(r - \frac{width}{2}\right) \cdot normalize\left(\mathbf{e}_n - (\mathbf{e}_n \cdot \mathbf{e}_{wheelAxis})\,\mathbf{e}_{wheelAxis}\right)}_{\mathbf{d}_1} \underbrace{- \frac{width}{2}\mathbf{e}_n}_{\mathbf{d}_2} \tag{2.5}$$

2.2.3 Voluminous wheel

The wheel is modelled as a voluminous wheel with a given radius r, a given width and a given curvature radius $r_{curvature}$. This object is an on both sides truncated torus with inner radius $r_i = r - r_{curvature}$ and $r_t = r_{curvature}$. The contact point is therefore located either on the torus surface or on one of the two edges confining the torus. If the inequality $|\mathbf{e}_{wheelAxis}\mathbf{e}_n r_{curvature}| > width/2$ is fulfilled the contact point lies on the edge.

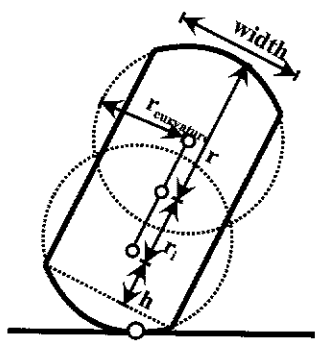

Figure 2.3: Geometry of a voluminous wheel

We state:

$$\mathbf{d}_{CP,0} = \underbrace{(r - r_{curvature}) \cdot normalize\left(\mathbf{e}_n - (\mathbf{e}_n \cdot \mathbf{e}_{wheelAxis})\,\mathbf{e}_{wheelAxis}\right)}_{\mathbf{d}_1} - \mathbf{d}_2 \tag{2.6}$$

where

$$\mathbf{d}_2 = \begin{cases} -\mathbf{e}_n r_{curvature} & |\mathbf{e}_{wheelAxis}\mathbf{e}_n r_{curvature}| \leq \frac{width}{2} \\ \pm\mathbf{e}_{wheelAxis}\frac{width}{2} + h\frac{d_1}{|d_1|} & |\mathbf{e}_{wheelAxis}\mathbf{e}_n r_{curvature}| > \frac{width}{2} \end{cases} \tag{2.7}$$

and

$$h = \sqrt{1 - \left(\frac{widht/2}{r_{curvature}}\right)^2}\, r_{curvature} \tag{2.8}$$

Chapter 3

Ideal rolling wheels (level 1)

On the first look a wheel or any other type of a rolling body doesn't differ much from a free body. It has a mass m, an inertia tensor $\mathbf{I}$ and it is accelerated by the gravity field with $\mathbf{g}_0$.

The body frame is given in the form of a coordinate system fixed to the wheel center, which is described by the positional vector $\mathbf{r}_0$ of the origin and the rotational matrix $\mathbf{R}$. The velocity $\mathbf{v}_0$ and acceleration $\mathbf{a}_0$ are resolved in the inertial frame, while ω and $\mathbf{z}$ are resolved in the body frame given by the rotational matrix $\mathbf{R}$, as well as the external force $\mathbf{f}$ and torque $\mathbf{t}$ acting on the center of the frame.

In addition the force $\mathbf{f}_{tyre,0}$ is acting on the contact point of the body. There is no torque acting on the contact point, because the contact region is assumed to be only a single point.

The basic mechanical equations hold with respect to the center of mass that is assumed to be at the wheel's center:

$$\mathbf{v}_0 = \dot{\mathbf{r}}_0 \tag{3.1}$$

$$\mathbf{a}_0 = \dot{\mathbf{v}}_0 \tag{3.2}$$

$$\mathbf{f} = m \cdot \mathbf{R}\left(\mathbf{a}_0 - \mathbf{g}_0 - \mathbf{f}_{tyre,0}\right) \tag{3.3}$$

$$\tilde{\omega}\mathbf{R} = \dot{\mathbf{R}} \tag{3.4}$$

with

$$\tilde{\omega} = \begin{pmatrix} 0 & -\omega_z & \omega_y \\ \omega_z & 0 & -\omega_x \\ -\omega_y & \omega_x & 0 \end{pmatrix} \tag{3.5}$$

$$\mathbf{z} = \dot{\omega} \tag{3.6}$$

$$\mathbf{t} = \mathbf{I}\mathbf{z} + \omega \times \mathbf{I}\omega + \mathbf{R}\left(\mathbf{d}_{CP,0} \times \mathbf{f}_{tyre,0}\right) \tag{3.7}$$

3.1 Holonomic and non-holonomic constraints

Unlike a free body, an ideal rolling body is bound on the rolling plane. This means, that the contact point $\mathbf{r}_{CP,0} = \mathbf{r}_0 + \mathbf{d}_{CP,0}$ has to be located on the plane, which leads to the holonomic constraint:

$$\mathbf{r}_{CP,0} \cdot \mathbf{e}_n = d; \tag{3.8}$$

The slip velocity is the velocity difference between the virtual contact point and the rolling plane. Because the rolling plane velocity is assumed to be zero, the velocity of the contact point equals the slip velocity. It can be decomposed into a lateral and a longitudinal component (both resolved in the inertial frame):

$$vSlip_{lat} = \left(\mathbf{v}_0 + \boldsymbol{\omega}_0 \times \mathbf{d}_{CP,0}\right) \cdot \mathbf{e}_{lat} \tag{3.9}$$

$$vSlip_{long} = \left(\mathbf{v}_0 + \boldsymbol{\omega}_0 \times \mathbf{d}_{CP,0}\right) \cdot \mathbf{e}_{long} \tag{3.10}$$

where $\boldsymbol{\omega}_0$ is the absolute angular velocity of the wheel resolved in the inertial frame. The additional unit vector $\mathbf{e}_{lat}$ results out of the projection of $\mathbf{e}_{wheelAxis}$ on the road plane.

$$\mathbf{e}_{lat} = normalize\left(\mathbf{e}_{wheelAxis} - (\mathbf{e}_{wheelAxis} \cdot \mathbf{e}_n)\mathbf{e}_n\right) \tag{3.11}$$

$$\mathbf{e}_{long} = \mathbf{e}_n \times \mathbf{e}_{lat}; \tag{3.12}$$

An ideal rolling body is by definition a body without slip. Therefore two non-holonomic constraints are introduced:

$$vSlip_{lat} = 0 \tag{3.13}$$

$$vSlip_{long} = 0 \tag{3.14}$$

$\mathbf{f}_{tyre,0}$ can be decomposed into f_n, f_{lat} and f_{long}:

$$\mathbf{f}_{tyre,0} = \mathbf{e}_n f_n + \mathbf{e}_{lat} f_{lat} + \mathbf{e}_{long} f_{long} \tag{3.15}$$

where f_n follows out of the holonomic constraint and f_{lat} and f_{long} are determined by the two non-holonimic constraints. The movement of the ideal rolling body is now completely defined.

Such a body has 5 degrees of freedom on positional level and 3 degrees of freedom on velocity level.

Chapter 4

Rigid wheels with slip (level 2)

The holonomic constraints are still maintained, even though such a wheel is allowed to take off the ground. However, to model the transition at collision time, force impulses are needed and this is tedious to define with the current version of Modelica.

Because slip is now allowed to happen, the two non-holonomic constraints are discarded and the forces f_{lat} and f_{long} are now a function of the total slip velocity $vSlip$:

$$vSlip = \left| vSlip_{lat}\, \mathbf{e}_{lat} + vSlip_{long}\, \mathbf{e}_{long} \right| = \left| \mathbf{v}_0 + \boldsymbol{\omega}_0 \times \mathbf{d}_{CP,0} \right| \tag{4.1}$$

The force is defined according to the basic law of friction:

$$\mathbf{f}_{friction} = -f_n\, \mu_{vSlip}\, \mathbf{e}_{vSlip} \tag{4.2}$$

where $\mathbf{e}_{vSlip}$ is a unit vector pointing in the direction of the slip velocity. The friction coefficient μ_{vSlip} is dependent on the total slip velocity $vSlip$ as shown by the solid characteristic curve in figure 4.1.

This friction force can be decomposed into a lateral and a longitudinal component resulting in equations for f_{lat} and f_{long}.

$$f_{lat} = -f_n\, \mu_{vSlip}\, \frac{vSlip_{lat}}{vSlip} \tag{4.3}$$

$$f_{long} = -f_n\, \mu_{vSlip}\, \frac{vSlip_{long}}{vSlip} \tag{4.4}$$

Such a wheel has now 5 degrees of freedom on positional and velocity level.

4.1 Behavior in adhesion

As simple as this might look, the situation gets difficult for small slip velocities in the case of adhesion. Unsurprisingly the system becomes very stiff for $vSlip$ close to zero, because a small change of the

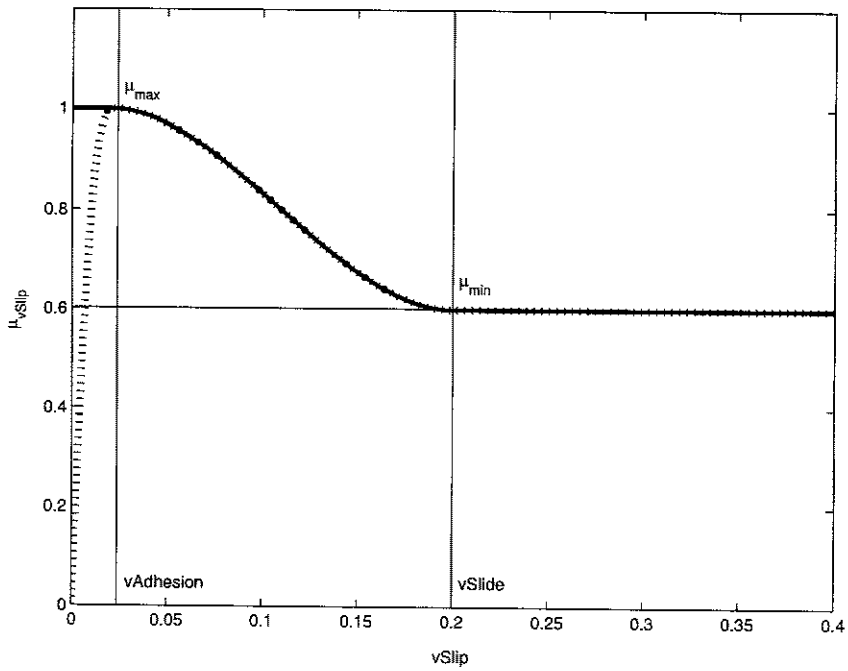

Figure 4.1: Characteristic curve of μ_{vSlip}. The solid line shows the correct dependence of the friction coefficient on the slip velocity. The dotted line was constructed to avoid difficulties (e.g. stiffness).

slip velocity leads to a drastic change of the force applied on the contact point. Also the slip velocity is very unlikely to become zero. Hence we are forced to establish a region of adhesion by defining a maximum adhesion velocity *vAdhesion*. It's usually set to a small arbitrary value (e. g. $1mm/s$).

If *vSlip* becomes smaller than *vAdhesion*, the wheel enters (according to the arbitrary definition above) the state of complete adhesion. Because of the numerical problems the non-zero slip velocities $vSlip_{lat}$ and $vSlip_{long}$ should now be set to zero by an artificial force impulse and the two non-holonomic constraints should be reestablished in the place of the equations 4.3 and 4.4 as long as f_{lat} and f_{long} don't exceed the limit given by $f_n\,\mu_{vSlip}(vSlip = 0)$. However this leads displeasingly to the need of impulse modelling and to awkward causality changes (The number of states is reduced in this stuck phase). Therefore an other pragmatic approach is preferred although it's incorrect for certain circumstances.

This simpler solution is achieved by sticking to equations 4.3 and 4.4 at all times and modify the characteristic curve of the friction for *vSlip* smaller than *vAdhesion*. This is indicated by the dotted line in figure 4.1.

This modified curve can roughly be described by the points $(vAdhesion, \mu_{max})$ and $(vSlide, \mu_{min})$. It crosses the origin with a slope $\dot{\mu}_{vSlip}(0)$ which is arbitrarily defined to be $\frac{2\mu_{max}}{vAdhesion}$. The complete curve

can be computed by using the following interpolation formula:

$$\mu_{vSlip} = \begin{cases} \dfrac{vSlip \cdot \dot{\mu}_{vSlip}(0)}{1+\sigma\left(\dfrac{vAdhesion}{\mu_{max}}\dot{\mu}_{vSlip}(0)-2+\sigma\right)} & vSlip \leq vAdhesion \\ & \sigma = \frac{vSlip}{vAdhesion} \\ \mu_{max}-(\mu_{max}-\mu_{min})\sigma^2(3-2\sigma) & vAdhesion < vSlip < vSlide \\ & \sigma = \frac{vSlip-vAdhesion}{vSlide-vAdhesion} \\ \mu_{min} & vSlide \leq vSlip \end{cases} \tag{4.5}$$

The derivative of this curve in respect to $vSlip$ is well defined at all points of the curve.

It is off course incorrect but very helpful, to have a characteristic friction curve crossing the origin with a slope $\dot{\mu}_{vSlip}(0)$. First of all this reduces the stiffness of the system and in addition it becomes evident by entering 4.5 into equation 4.3 for $vSlip < vAdhesion$ that $vSlip$ can be abbreviated:

$$f_{lat} = f_n \mu_{vSlip} \frac{vSlip_{lat}}{vSlip} \tag{4.6}$$

$$= f_n \frac{vSlip \cdot \dot{\mu}_{vSlip}(0)}{1+\sigma\left(\dfrac{vAdhesion}{\mu_{max}}\dot{\mu}_{vSlip}(0)-2+\sigma\right)} \frac{vSlip_{lat}}{vSlip} \tag{4.7}$$

$$= f_n \frac{\dot{\mu}_{vSlip}(0)}{1+\sigma\left(\dfrac{vAdhesion}{\mu_{max}}\dot{\mu}_{vSlip}(0)-2+\sigma\right)} vSlip_{lat} \tag{4.8}$$

This solves the numerical problem for small slip velocities, that would occur otherwise. Therefore, $\frac{\mu_{vSlip}}{vSlip}$ is computed directly and the equations 4.3 and 4.4 change to

$$f_{lat} = f_n \left(\frac{\mu_{vSlip}}{vSlip}\right) vSlip_{lat} \tag{4.9}$$

$$f_{long} = f_n \left(\frac{\mu_{vSlip}}{vSlip}\right) vSlip_{long} \tag{4.10}$$

This solution is fully sufficient for most of the cases, but it is a bad solution for static problems. Imagine a car just recently parked on an uphill road. It would then start to slide downwards, very slowly but very certainly.

Chapter 5

Wheels with simple slick tyre (level 3)

The model sketched above can easily be enhanced to a freely moving wheel with a simply elastic tyre. The tyre is modelled by a virtual spring damper system as sketched in figure 5.1.

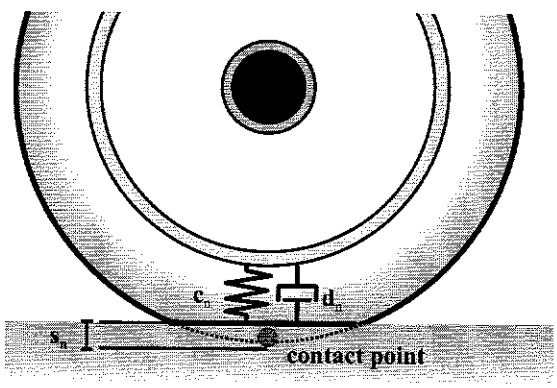

Figure 5.1: The deformation of the tyre in direction of the road normal is modelled with a virtual spring damper element.

The holonomic constraint 3.8 is discarded and the equation 3.8 changes into:

$$(\mathbf{r}_0 + \mathbf{d}_{CP,0}) * \mathbf{e}_n = d + s_n \tag{5.1}$$

where s_n is the travel of the virtual tyre spring and in consequence:

$$f_n = \begin{cases} -min(0, c_n s_n + d_n \dot{s_n}) & if\ s_n < 0 \\ 0 & else \end{cases} \tag{5.2}$$

where c_n and d_n denote the spring and damping constant. This is introducing no additional state variable, because s_n and $\dot{s_n}$ are computed out of the wheels position and velocity.

Furthermore the force $\mathbf{f}_{tyre}$ acts now on the projection of the virtual contact point on the road. Therefore the equation 3.7 is modified:

$$\mathbf{t} = \mathbf{I}\mathbf{z} + \boldsymbol{\omega} \times \mathbf{I}\boldsymbol{\omega} + \mathbf{R}\left(\mathbf{d}_{CP,0} - s_N \cdot \mathbf{e}_N \times \mathbf{f}_{tyre,0}\right) \tag{5.3}$$

Chapter 6

Modelling of a tyre with tread (level 4)

So far the contact between road and wheel was modelled by a single point. In consequence only forces and no torques are applied on the contact point.

To develop a more realistic model of a wheel, we take a closer look on what happens in the contact region between road and tyre. As can be seen in figure 6.1 the area of contact is now modelled by a region or tread shuffle surrounding the contact point with a certain length l_{CR} and a certain width w_{CR}.

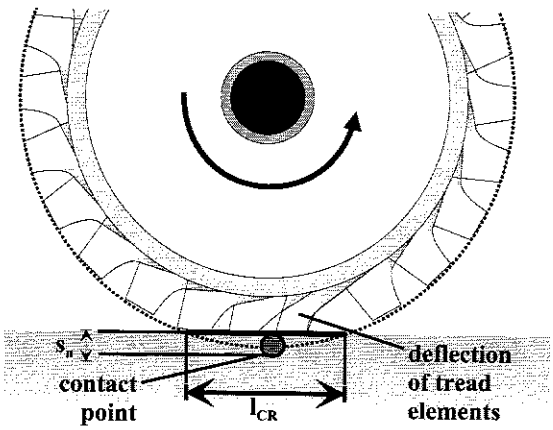

Figure 6.1: An Illustration of the tread element's deflection within the contact area (marked by l_{CR}).

The dependence of l_{CR} on s_n can be approximated for wheels with radius r:

$$l_{CR} = \sqrt{8rs_n}\,^{1} \tag{6.1}$$

Equations for the width w_{CR} can be derived in dependence on the wheel geometry by using the same

[1] this approximation follows out of pythagoras' rule $\left(\frac{l_{CR}}{2}\right)^2 = r^2 - (r - s_n)^2$ for $s_n \ll r$

approximation scheme.

$$w_{CR} = \begin{cases} width & \texttt{flat disc} \\ \sqrt{4 width\, s_n} & \texttt{torus} \\ \sqrt{8 r_{curvature} s_n} & \texttt{vol. wheel} \end{cases} \tag{6.2}$$

Bristles or tread elements are placed on the tyre surface, forming the tread pattern. These little parts undergo a deflection in the tread shuffle. This deflection can be computed out of the slip velocity $vSlip$, given the approximated time t_{CR} of a particle to stay in the contact region t_{CR}.

$$\texttt{max. particle deflection} = vSlip * t_{CR} \tag{6.3}$$

$$= vSlip \frac{l_{CR}}{|\mathbf{d}_{CP,0} \times \omega_0)|} \tag{6.4}$$

$$= vSlip \frac{l_{CR}}{vRoll} \tag{6.5}$$

As can be seen out of these equations t_{CR} is computed by dividing the length of the tread shuffle with the velocity of a tread element travelling through it. This velocity is denoted as the roll velocity $vRoll$.

The slip S (not to confuse with the slip velocity $vSlip$!) is defined to be a dimensionless number proportional to the particle deflection. Therefore:

$$S = \frac{vSlip}{vRoll} \tag{6.6}$$

and ...

$$S_{lat} = vSlip_{lat}/vRoll \tag{6.7}$$

$$S_{long} = vSlip_{long}/vRoll \tag{6.8}$$

respectively.

Given the presumption that the bristles adhere ($S < sAdhesion$), it is assumed that the force applied on the wheel is proportional to the bristle's deflection and therefore also proportional to the slip S. If the maximum slip $sAdhesion$ is exceeded, the tread elements start to slide and less force is transmitted until the state of total sliding $sSlide$ is reached. Hence we expect an dependence of the friction coefficient μ_S on the slip S like it is shown by the characteristic curve in figure 6.2.

Again this curve can roughly be described by two points: $(sAdhesion, \mu_{max})$ and $(sSlide, \mu_{min})$. It also crosses the origin with a slope $\mu_S(0)$ which is arbitrarily defined to be $2 * \mu_{max}/sAdhesion$. The formula 4.5 can afresh be applied for the interpolation.

This characteristic curve is also dependent on the direction of the slip. This can be achieved by defining two separate characteristic curves for lateral and longitudinal direction with two pairs:

$$[(sAdhesionLat, \mu_{max,lat}), (sSlideLat, \mu_{min,lat})]$$

$$[(sAdhesionLong, \mu_{max,long}), (sSlideLong, \mu_{min,long})]$$

and mixing these parameters according to the trigonometric pythagoras:

$$sAdhesion = \sqrt{\left(\frac{vSlip_{lat}}{vSlip}\right)^2 sAdhesion_{lat}^2 + \left(\frac{vSlip_{long}}{vSlip}\right)^2 sAdhesion_{long}^2} \tag{6.9}$$

$$sSlide = \sqrt{\left(\frac{vSlip_{lat}}{vSlip}\right)^2 sSlide_{lat}^2 + \left(\frac{vSlip_{long}}{vSlip}\right)^2 sSlide_{long}^2} \tag{6.10}$$

and just as well for μ_{max} and μ_{min}:

$$\mu_{max} = \sqrt{\left(\frac{vSlip_{lat}}{vSlip}\right)^2 \mu_{max,lat}^2 + \left(\frac{vSlip_{long}}{vSlip}\right)^2 \mu_{max,long}^2} \tag{6.11}$$

$$\mu_{min} = \sqrt{\left(\frac{vSlip_{lat}}{vSlip}\right)^2 \mu_{min,lat}^2 + \left(\frac{vSlip_{long}}{vSlip}\right)^2 \mu_{min,long}^2} \tag{6.12}$$

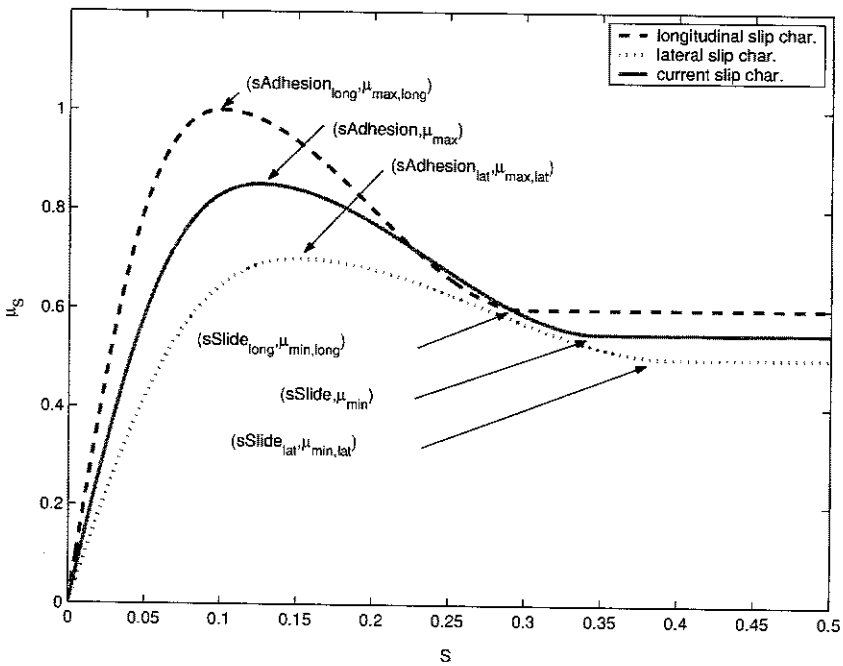

Figure 6.2: Characteristic curves for μ_S. At the beginning they all raise linearly, until the tread elements start to slide. The dashed blue curve shows the characteristics for pure lateral slip. The behavior for pure longitudinal slip is presented by the dotted green curve. Hence the actual characteristic curve is dependent on the slip direction and can be approximated for a certain case by mixing the four parameters as shown be the solid red showcase curve.

Although the slip is an excellent variable to find a good description of the tyre behavior in most of the relevant cases, its usage is unfortunately incorrect for small rolling velocities. To examine and eliminate this problem the dependence of μ_S on $vSlip$ and $vRoll$ is regarded. Figure 6.3(a) shows this dependency which follows out of the relation:

$$\mu_S = func(S) = func\left(\frac{vSlip}{vRoll}\right)$$

For small values of *vRoll* the characteristic curve collapses and μ_S is μ_{min} for almost all values of *vSlip*. This is completely wrong if the wheel is rolling slowly or standing still. μ_S should be close to μ_{max} in such a situation.

Figure 6.3(b) shows the characteristic curve of μ_S as described in section 4.

$$\mu_S = func(vSlip)$$

This is a correct behavior for low rolling velocities, but discards the effect of slip due to the bristle deflection completely.

The goal is, off course, to combine the best of both. This is achieved by making the parameters of the curve in figure 4.1 dependent on *vRoll*. The original values for *vAdhesion* and *vSlide* are replaced by *vAR* and *vSR*

$$vAR = softmax_{tol}(vAdhesion, sAdhesion \cdot vRoll) \tag{6.13}$$

$$vSR = softmax_{tol}(vSlide, sSlide \cdot vRoll) \tag{6.14}$$

where

$$softmax_{tol}(a,b) = log\left(e^{a/tol} + e^{b/tol}\right) \cdot tol \tag{6.15}$$

The Influence of *vSlip* on the friction coefficient mu_S is modelled according to the equation 4.1:

$$\mu_S = \begin{cases} \dfrac{vSlip \cdot \dot{\mu}_{vSlip}(0)}{1+\sigma\left(\dfrac{vAR}{\mu_{max}}\dot{\mu}_{vSlip}(0) - 2 + \sigma\right)} & vSlip \leq vAR \\ & \sigma = \frac{vSlip}{vAR} \\ \mu_{max} - (\mu_{max} - \mu_{min})\sigma^2(3-2\sigma) & vAR < vSlip < vSR \\ & \sigma = \frac{vSlip - vAR}{vSR - vAR} \\ \mu_{min} & vSR \leq vSlip \end{cases} \tag{6.16}$$

The final result is shown in figure 6.3(c).

6.1 Non-linear influence of the normal load

So far all friction forces (f_{lat} and f_{long}) were assumed to be linear dependent on the normal load f_n, but the stiffness of the tyre leads to a non-uniform pressure distribution in the tread shuffle. At the entrance and at the exit of the tread shuffle the pressure is too low to deflect the tread elements. A potential pressure peak in the front part of the shuffle can't effectively transmit the force because of the tread elements' low deflection at that position.

Therefore the transmitted friction forces are increasing less than linear in respect to the normal load. To model this non-linearity the friction coefficients are dependent on f_n

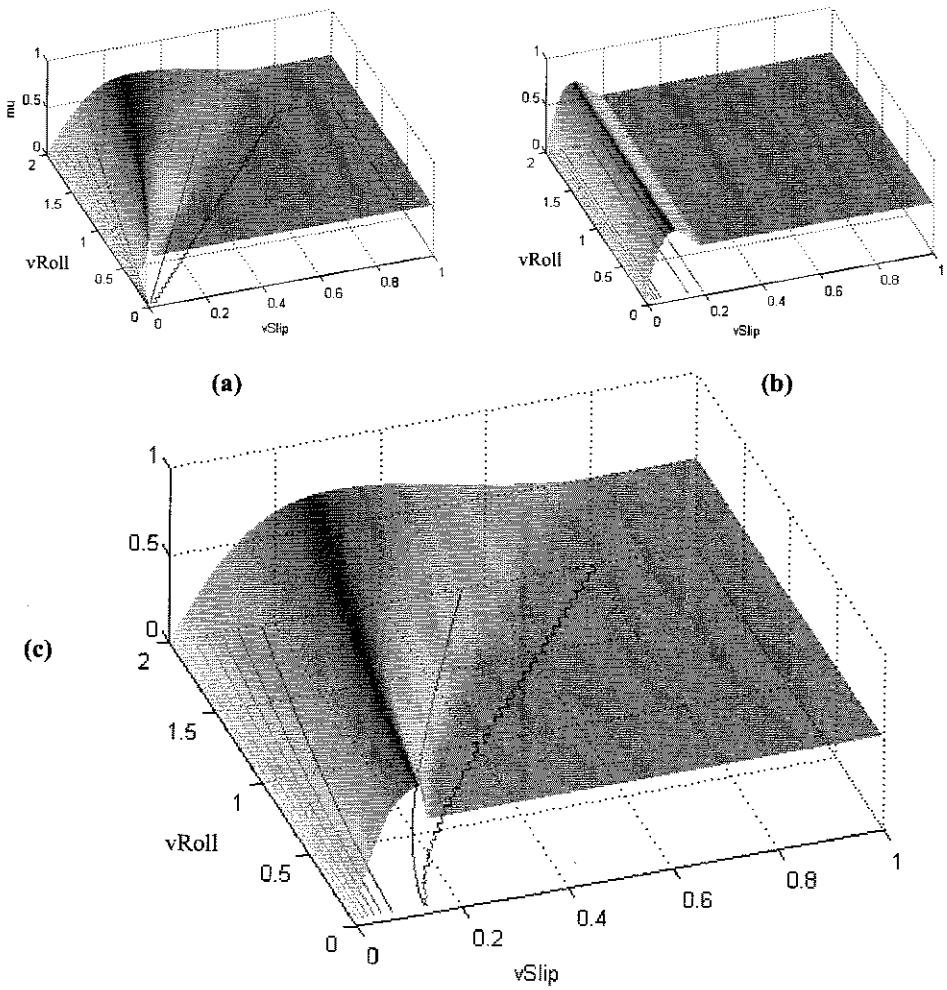

Figure 6.3: Characteristic surfaces of the friction coefficient in dependence of v_{Roll} and $vSlip$ In (a) the surface is solely defined by the slip whereas in(b) the dependency is purely on the slip velocity. The actual characteristic (c) results out of a combination of (a) and (b)

Given two values for a friction coefficient μ: μ_1 and μ_2 at $f_n = f_{n,1}$ and $f_n = f_{n,2} = 2f_{n,1}$ the non-linearity can be captured with a linear decreasing $\mu(f_n)$.

$$\mu = (2\mu_1 - \mu_2) - (\mu_1 - \mu_2)\frac{f_n}{f_{n,1}} \tag{6.17}$$

The resulting friction force $f_n \cdot \mu$ is then a quadratic function of f_n with a peak at:

$$f_n = f_{n,sat} = \frac{f_{n,1}(2\mu_1 - \mu_2)}{2(\mu_1 - \mu_2)} \tag{6.18}$$

For all $f_n > f_{n,sat}$ the friction force is the maximal force at the peak and the coefficient μ is:

$$\mu = \frac{(2\mu_1 - \mu_2)^2}{4(\mu_1 - \mu_2)}\frac{f_{n,1}}{f_n} \tag{6.19}$$

We define the friction coefficients $\mu_{max,lat}$, $\mu_{max,long}$, $\mu_{min,lat}$, $\mu_{min,long}$ and μ_{turn}(will appear later) to be dependent on f_n as sketched in equations 6.17 and 6.19.

Also the parameters $sSlide_{lat}$, $sAdhesion_{lat}$, $sSlide_{long}$ and $sAdhesion_{long}$ are assumed to be linear dependent on the normal load. Having given all these values at $f_n = f_{n,1}$ and $f_n = 2f_{n,1}$ the dependency can simple be modelled by a linear approximation as in equation 6.17.

6.2 Lateral slip due to camber angle

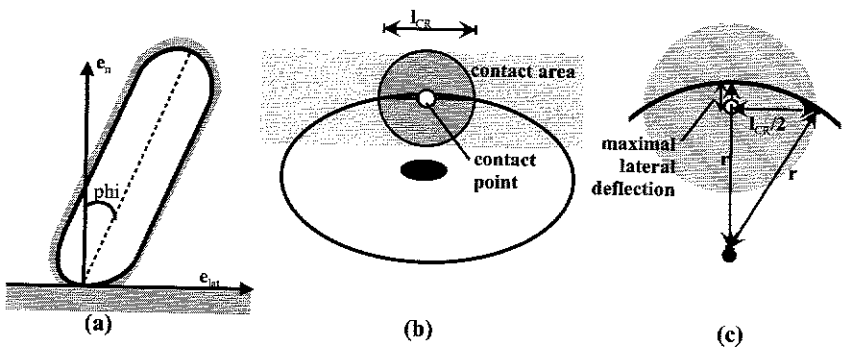

Figure 6.4: Different views of a tilted wheel: (a) side view, (b) top view. (c) shows a magnification of (b) whereas the wheel lies on the plane.

Figure 6.4(a) shows a tilted wheel with a camber angle phi. A tread element of a wheel in such a position would like to make a curve by going through the contact region and is therefore deflected in lateral direction. Figure 6.4(b) illustrates this by a view from above. Hence, the influence of camber can be fairly modelled by the adding of a lateral slip: the camber slip. To compute this, an estimation of the maximum lateral deflection due to camber is needed:

$$maxCamberDefl = r - r\sqrt{1 - \left(\frac{l_{CR}}{2r}\right)^2} \tag{6.20}$$

This formula can be extracted out of figure 6.4(c) by the use of trigonometry.

The actual deflection is then

$$camberDefl = sin(phi) \cdot maxCamberDefl \tag{6.21}$$

and the resulting lateral slip velocity is:

$$camberVSlip = vRoll \cdot gain_{camber} \cdot camberDefl \tag{6.22}$$

where $gain_{camber}$ is a parameter needed to transform the deflection into the dimensionless slip. It must be found by measurement.

In consequence equation 3.12 changes into

$$vSlip_{lat} = \left(\mathbf{v}_0 + \omega_0 \times \mathbf{d}_{CP,0}\right) \cdot \mathbf{e}_{lat} + camberVSlip \tag{6.23}$$

6.3 Influence of trail

The pressure distribution of the tyre in the tread shuffle changes dependent on the driving situations. The pressure peak is usually longitudinal behind the contact point by normal adhesive rolling. In the transition between rolling and sliding it moves in front of the contact point and becomes equal to contact point in the case of complete slip.

This positional shift of the pressure peak is denoted by l_{trail} and can be found with the following empiric formula[1]:

$$l_{trail} = \begin{cases} \frac{1}{6} l_{CR} \left(1 - \frac{vSlip_{lat}}{vAR}\right) & vSlip_{lat} \leq vAR \\ \frac{-1}{6} l_{CR} \dfrac{vSlip_{lat} - vAR}{vAR \left(\frac{vSR - vSlip_{lat}}{vSR - vAR}\right)^2} & vAR < vSlip_{lat} < vSR \\ 0 & vSR \geq vSlip_{lat} \end{cases} \tag{6.24}$$

The lateral force f_{lat} acts at this pressure peak, not at the contact point and therefore causes a torque in the direction of e_n.

$$\mathbf{t}_{TB} = gain_{TB} \left(-sign_{trail}\, l_{trail}\, \mathbf{e}_{long} \times f_{lat} \mathbf{e}_{lat}\right) \tag{6.25}$$

where $gain_{TB}$ is a parameter to model the strength of this effect and where signTrail*eLong points into the direction of the rolling and thus $sign_{trail}$ could be computed with

$$sign_{trail} = sign\left((\omega_0 \times \mathbf{r}_{CP,0}) \cdot \mathbf{e}_{long}\right) \tag{6.26}$$

to avoid a possible stiffness it is better to use a continuous formulation like:

$$sign_{trail} = \begin{cases} sign\left((\omega_0 \times \mathbf{r}_{CP,0}) \cdot \mathbf{e}_{long}\right) & (\omega_0 \times \mathbf{r}_{CP,0}) \cdot \mathbf{e}_{long} > vAdhesion \\ (\omega_0 \times \mathbf{r}_{CP,0}) \cdot \frac{\mathbf{e}_{long}}{vAdhesion} & else \end{cases} \tag{6.27}$$

6.4 Roll resistance and turning friction

The angular velocity w_0 of the wheel is decomposed into a rolling part w_{roll} and a turning part w_{turn}:

$$\omega_{turn} = (\omega_0 \cdot \mathbf{e}_n) \cdot \mathbf{e}_n \tag{6.28}$$

$$\omega_{roll} = \omega_0 - \omega_{turn} \tag{6.29}$$

Roll resistance is denoting a phenomenon which is a summarization of numerous effects. One source of rolling resistance is the imperfect elastic deformation of the tyre, which results in a loss of energy. In a rolling wheel there is also an agglomeration of air at the entrance of the tread shuffle that needs to be pushed around the rim while driving. This pressure peak at the shuffle entrance is also causing a counteracting momentum.

In contrast to the complex effects underlying the phenomenon of rolling resistance there is the simplicity of the usual description by a single coefficient: μ_{roll}. This coefficient is usually given in a way that the imaginary counteracting force acting at the wheel center is $f_n \cdot \mu_{roll}$.

Here the counteracting torque is preferred, which leads to the multiplier r:

$$|\mathbf{t}_{roll}| = f_n \cdot r \cdot \mu_{roll} \tag{6.30}$$

This equation holds if the wheel is rolling. For the sake of simplicity the transition between rolling and still standing is described by the simplest possible characteristic curve. See figure 6.5

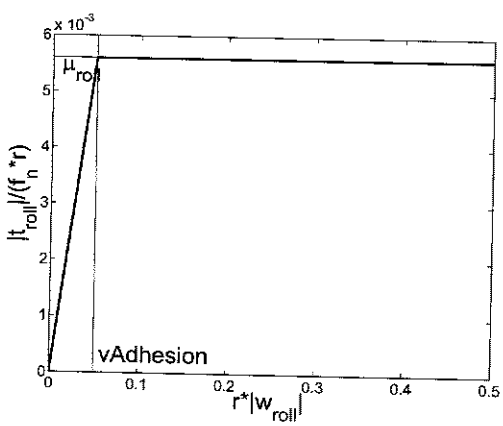

Figure 6.5: Characteristic curve of the roll resistance torque.

The resulting torque points in the negative direction of w_{roll}:

$$-\mathbf{t}_{roll} = \begin{cases} f_n \mu_{roll} r \frac{\omega_{roll}}{|\omega_{roll}|} & r|\omega_{roll}| > vAdhesion \\ f_n \mu_{roll} r^2 \frac{\omega_{roll}}{vAdhesion} & r|\omega_{roll}| \leq vAdhesion \end{cases} \tag{6.31}$$

This model of the rolling resistance might be a bit too simple. Some sources [7], [8] state that the coefficient is rising linearly or quadratically with the wheel's velocity. Anyhow for high speeds the air resistance usually becomes the major loss of energy by far and the influence of rolling resistance often becomes almost negligible.

Although the rolling resistance could not convincingly be introduced until this level of complexity, it has been implemented in the same way for all levels from level 2 on.

The turning resistance is dependent on the roll velocity as one can clearly experience in an old car without servo steering. All the tread elements in the contact region are deflected by turning the wheel. This deflection is proportional to the distance to the contact point, as illustrated in figure 6.6.

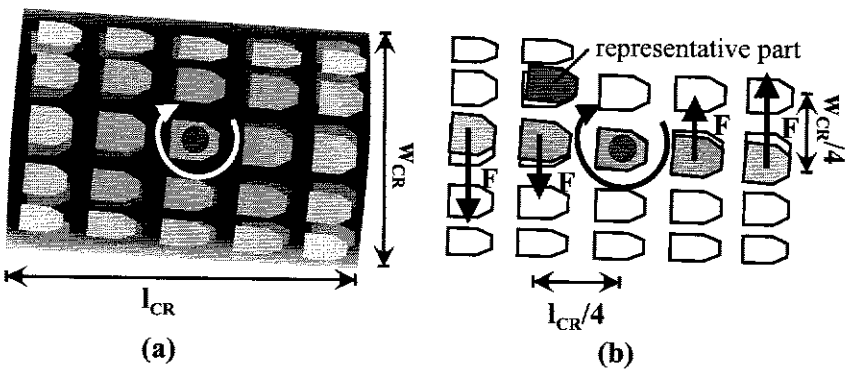

Figure 6.6: The two plan views of the contact region show the deflection of the tread elements due to the turning of the wheel. In (b) the representative part is marked and the forces on the single tread elements are drawn.

Because it is presumed that the resulting force on the tread elements is proportional to deflection and therefore proportional to the slip, the resulting torque can sufficiently be modelled by computing the slip of a single representative tread element. This will be shown more clearly in the following paragraphs:

The slip of a tread element with distance $s = \sqrt{x^2+y^2}$ to the contact point is $|\omega_{turn}|\, s \cdot sAdhesion/vAR$. Again for the sake of simplicity the characteristic curve of the friction coefficient just models a limited proportionality. See figure 6.7. The resulting force on such an element is then:
$min\left(f_n\, \mu_{turn}\, |\omega_{turn}|\, s/vAR, f_n\, \mu_{turn}\right)$

The overall torque $|t_{turn}|$ results of the summation of the forces on all the tread elements. We assume

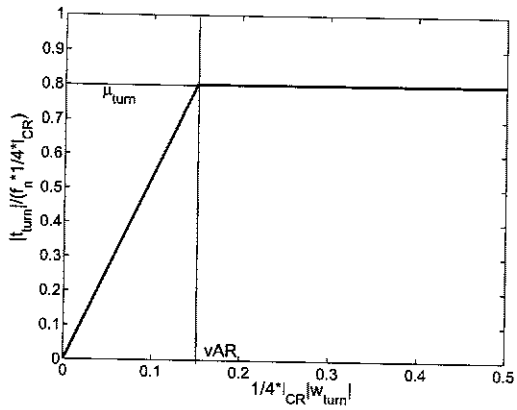

Figure 6.7: Characteristic curve of turning friction torque

that $|w_{turn}|s$ is always smaller than vAR:

$$|\mathbf{t}_{turn}| = \int_{-l_{CR}/2}^{l_{CR}/2}\int_{-w_{CR}/2}^{w_{CR}/2} s\frac{f_n}{l_{CR}w_{CR}}\mu_{turn}\frac{|\omega_{turn}|}{vAR}s\,dy\,dx \tag{6.32}$$

$$|\mathbf{t}_{turn}| = \frac{4}{l_{CR}w_{CR}}f_n\,\mu_{turn}\frac{|\omega_{turn}|}{vAR}\int_0^{l_{CR}/2}\int_0^{w_{CR}/2} s^2\,dy\,dx \tag{6.33}$$

$$|\mathbf{t}_{turn}| = \frac{4}{l_{CR}w_{CR}}f_n\,\mu_{turn}\frac{|\omega_{turn}|}{vAR}\int_0^{l_{CR}/2}\int_0^{w_{CR}/2} (x^2+y^2)\,dy\,dx \tag{6.34}$$

$$|\mathbf{t}_{turn}| = \frac{1}{12}(l_{CR}^2+w_{CR}^2)f_n\,\mu_{turn}\frac{|\omega_{turn}|}{vAR} \tag{6.35}$$

The result can be rearranged:

$$|\mathbf{t}_{turn}| = \sqrt{\left(\sqrt{\frac{l_{CR}}{12}}\right)^2+\left(\sqrt{\frac{w_{CR}}{12}}\right)^2}\,f_n\,\mu_{turn}\frac{|\omega_{turn}|\sqrt{\left(\sqrt{\frac{l_{CR}}{12}}\right)^2+\left(\sqrt{\frac{w_{CR}}{12}}\right)^2}}{vAR} \tag{6.36}$$

$$|\mathbf{t}_{turn}| \approx \frac{1}{4}\sqrt{l_{CR}^2+w_{CR}^2}f_n\,\mu_{turn}\frac{|\omega_{turn}|\frac{1}{4}\sqrt{l_{CR}^2+w_{CR}^2}}{vAR} \tag{6.37}$$

It has now become obvious that $\mathbf{t}_{turn}$ can approximately be obtained by computing the torque on a single representative part with distance $s \approx \frac{1}{4}\sqrt{l_{CR}^2+w_{CR}^2}$ to the contact point.

$$-\mathbf{t}_{turn} = \begin{cases} \hat{f}_n\,\mu_{turn}\frac{1}{16}\left(l_{CR}^2+w_{CR}^2\right)\frac{\omega_{turn}}{vAR} & |\omega_{turn}|\frac{1}{4}\sqrt{l_{CR}^2+w_{CR}^2} \le vAR \\ \hat{f}_n\,\mu_{turn}\frac{1}{4}\sqrt{l_{CR}^2+w_{CR}^2}\frac{\omega_{turn}}{|\omega_{turn}|} & |\omega_{turn}|\frac{1}{4}\sqrt{l_{CR}^2+w_{CR}^2} > vAR \end{cases} \tag{6.38}$$

Chapter 7

Implicit modelling of the tyre deformation (level 5 and 6)

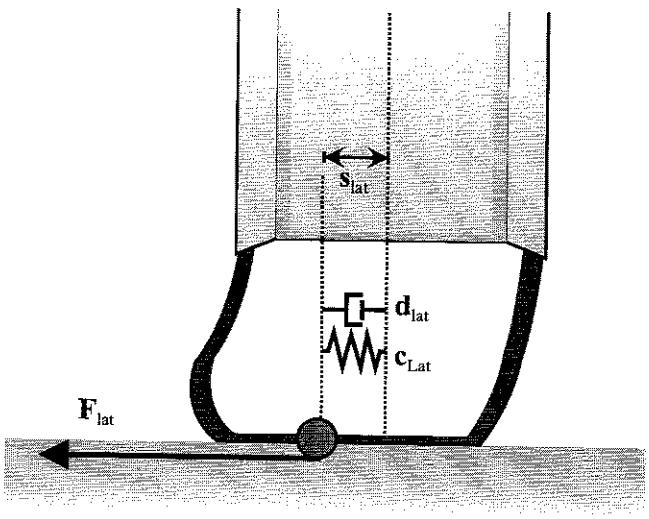

Figure 7.1: The lateral deformation of a tyre is modelled again with a spring damper system

The lateral deformation of the tyre can be modelled with a virtual spring damper system, as presented in figure 7.1. The spring travel is denoted with s_{lat} and depends on the lateral force f_{lat}:

$$f_{lat} = c_{lat} s_{lat} + d_{lat} \dot{s}_{lat} \tag{7.1}$$

where c_{lat} and d_{lat} are the spring and damping constants.

The lateral deformation influences the slip velocity and therefore the equation 6.23 (and 3.12 respectively) is changed again:

$$(\mathbf{v}_0 + \omega_0 \times \mathbf{d}_{CP,0}) \cdot \mathbf{e}_{lat} + camberVSlip = vSlip_{lat} - \dot{s}_{lat} \tag{7.2}$$

The same can be done for a longitudinal deformation:

$$f_{long} = c_{long} s_{long} + d_{long} \dot{s}_{long} \tag{7.3}$$

$$(\mathbf{v}_0 + \omega_0 \times \mathbf{d}_{CP,0}) \cdot \mathbf{e}_{long} + camberVSlip = vSlip_{long} - \dot{s}_{long} \tag{7.4}$$

To run this system two non-linear equations have to be solved. This is usually not a problem for today's simulation programs (e. g. Dymola). Anyhow one might still be interested in a linearized solution.

7.1 Linearized solution (level 5)

To remove the to nonlinear equations we linearize at the point of the static solution $\dot{s}_{Lat} = 0$.

$$f_{lat} = f_{lat}|_{\dot{s}_{lat}=0} + \left.\frac{df_{lat}}{d\dot{s}_{lat}}\right|_{\dot{s}_{lat}=0} \cdot \dot{s}_{lat} \tag{7.5}$$

and inserting this into equation 7.1 leads to:

$$f_{lat}|_{\dot{s}_{lat}=0} = c_{lat} s_{lat} + \underbrace{\left(d_{lat} - \left.\frac{df_{lat}}{d\dot{s}_{lat}}\right|_{\dot{s}_{lat}=0} \right)}_{D} \cdot \dot{s}_{lat} \tag{7.6}$$

Because $f_{lat}|_{\dot{s}_{lat}=0}$ can be computed with the aid of $vSlip_{lat}|_{\dot{s}_{lat}=0}$, this equation is used to find a good estimate for $\dot{s}_{lat}$.

But first we need to derive $\left.\frac{df_{lat}}{d\dot{s}_{lat}}\right|_{\dot{s}_{lat}=0}$:

$$\frac{df_{lat}}{d\dot{s}_{lat}} = \frac{d\left(f_n \mu_{vSlip} \frac{vSlip_{lat}}{vSlip}\right)}{d\dot{s}_{lat}} \tag{7.7}$$

$$= f_n \frac{vSlip_{lat}}{vSlip} \frac{d\mu_{vSlip}}{d\dot{s}_{lat}} + \underbrace{f_n \mu_{vSlip}}_{\sqrt{f_{lat}^2 + f_{long}^2}} \frac{d\frac{vSlip_{lat}}{vSlip}}{d\dot{s}_{lat}} \tag{7.8}$$

$$= -f_n \frac{vSlip_{lat}}{vSlip} \frac{d\mu_{vSlip}}{dvSlip} \underbrace{\frac{dvSlip}{d\dot{s}_{lat}}}_{\frac{vSlip_{lat}}{vSlip}} + \sqrt{f_{lat}^2 + f_{long}^2} \frac{d\frac{vSlip_{lat}}{vSlip}}{d\dot{s}_{lat}} \tag{7.9}$$

$$= -f_n \left(\frac{vSlip_{lat}}{vSlip}\right)^2 \frac{d\mu_{vSlip}}{dvSlip} - \sqrt{f_{lat}^2 + f_{long}^2} \frac{vSlip - \frac{vSlip_{lat}^2}{vSlip}}{vSlip^2} \tag{7.10}$$

$$= -f_n \left(\frac{vSlip_{lat}}{vSlip}\right)^2 \frac{d\mu_{vSlip}}{dvSlip} - \sqrt{f_{lat}^2 + f_{long}^2} \frac{\left(\frac{vSlip_{long}}{vSlip}\right)^2}{vSlip} \tag{7.11}$$

$\frac{d\mu_{vSlip}}{dvSlip}$ can be found by taking the derivative of equation 4.5, but one has to be careful that $D = d_{lat} - \frac{df_{lat}}{d\dot{s}_{lat}}\Big|_{\dot{s}_{lat}=0}$ doesn't become negative for $vSlip_{lat} > vAR$. Hence $\frac{d\mu_{vSlip}}{dvSlip}$ is artificially bound to positive values. This leads to an incorrect (but at least good natured) behavior in the transition phase between adhesion and slide.

$\dot{s}_{lat}$ can now be computed using the equation 7.6.

$\dot{s}_{long}$ can be derived similarly using the equations:

$$f_{long}\big|_{\dot{s}_{long}=0} = c_{long}s_{long} + \left(d_{long} - \frac{df_{long}}{d\dot{s}_{long}}\Big|_{\dot{s}_{long}=0}\right) \cdot \dot{s}_{long} \tag{7.12}$$

$$\frac{df_{long}}{d\dot{s}_{long}} = -f_n \left(\frac{vSlip_{long}}{vSlip}\right)^2 \frac{d\mu_{vSlip}}{dvSlip} - \sqrt{f_{lat}^2 + f_{long}^2}\frac{\left(\frac{vSlip_{lat}}{vSlip}\right)^2}{vSlip} \tag{7.13}$$

Once $\dot{s}_{lat}$ and $\dot{s}_{long}$ are known, f_{lat} and f_{long} can be computed via $vSlip_{lat}$ and $vSlip_{long}$ using the equations 7.2 and 7.4.

Chapter 8

Explicit modelling of the tyre deformation (level 7)

The solution in the last chapter only modelled the influence of the deformation on the slip velocity, the actual shift of the contact point was not taken into account. Thus we say that the deformation of the tyre was only implicitly modelled. An explicit modelling can be achieved by decomposing the wheel into two idealized parts: The rim and the tyre.

The rim has all the mass and inertia, the tyre is massless and determines the forces acting on it according to its position and velocity. The rim and the tyre are connected with two prismatic spring damper joints in longitudinal and lateral direction (again specified by c_{long}, d_{long} , c_{lat}, d_{lat}).

To achieve this decomposition it is fully sufficient to introduce two new variables, which replace $\mathbf{r}_0$ and $\mathbf{v}_0$ for the tyre component: $\mathbf{rb}_0$ and $\mathbf{vb}_0$.

$$\mathbf{rb}_0 = \mathbf{r}_0 + s_{lat}\mathbf{e}_{lat} + s_{long}\mathbf{e}_{long} \tag{8.1}$$

$$\mathbf{vb}_0 = \dot{\mathbf{rb}}_0 \tag{8.2}$$

All the occurrences of $\mathbf{r}_0$ and $\mathbf{v}_0$ in the equations concerning contact point finding and slip velocity have to be replaced with $\mathbf{rb}_0$ and $\mathbf{vb}_0$.

To model the spring damper system we use again the equations 7.1 and 7.3.

From the equations for the body dynamics 3.3 and 5.3 only the equation concerning the torque is modified:

$$\mathbf{t} = \mathbf{I}\cdot\mathbf{z} + (\omega \times \mathbf{I}\cdot\omega) + \mathbf{R}\left(\left(\mathbf{rb}_0 - \mathbf{r}_0 + \mathbf{d}_{CP,0} - s_N\cdot\mathbf{e}_N\right)\times\mathbf{f}_{tyre,0}\right) \tag{8.3}$$

Again two non-linear equations have to be solved to simulate this model.

Chapter 9

Handling of uneven terrain

It might be interesting to let a wheel roll on an uneven terrain, not only on a straight plane.

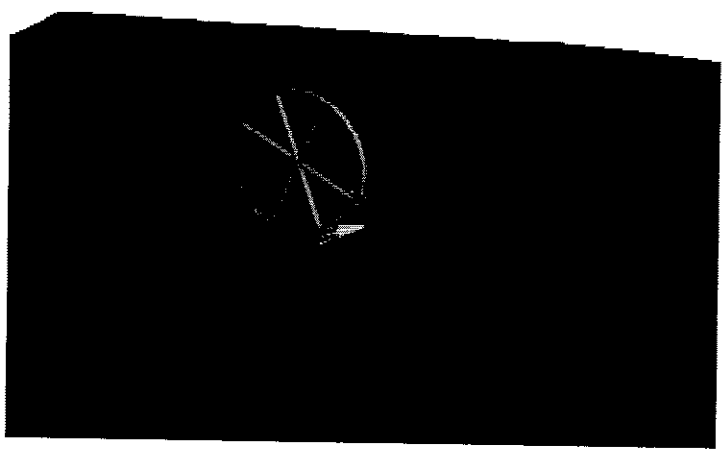

Figure 9.1: a wheel rolling over a hump

9.1 An uneven road as parametric surface

The implementation of uneven terrain and the calculation of several possible contact points is a non-trivial problem in general[5]. To avoid an excess of complexity for the total model a simpler solution is provided, making a few helpful (but also restricting) assumptions:

- The road is given in the inertial frame by a parametric surface $f(x,y)$ with $x = x$ and $y = y$ and

$z = f(x,y)$ and for all points on the road plane the normal vector is well defined.

- The road's curvature is always significantly weaker then the curvature of the wheel. This means: There is always just a single contact point.
- The road is not too steep. $\frac{dz}{dx}$ and $\frac{dz}{dy}$ should not excess the value 1.

Therefore the road can simply be modelled by changing the parameters $\mathbf{e}_n$ and d into functions of x and y. To describe the uneven road a topographic map is used. The values for z, dz/dx and dz/dy are given at certain sampling points placed on a regular grid in the xy-plane. All z values between the grid are interpolated using bicubic polynoms[3]. The interpolation scheme is presented by an easy example, where all four sampling points are placed on a unit square.

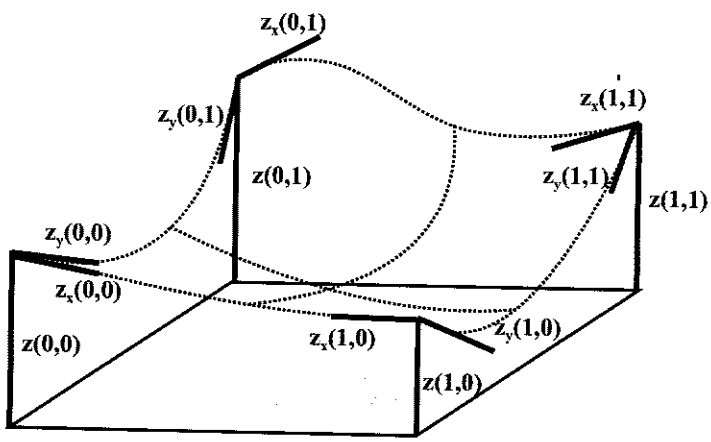

Figure 9.2: The z-values and the their derivatives are given at the points of a unit square in the xy-plane. The resulting interpolated surface is sketched with dashed lines.

Given the situation of figure 9.2 the z-values can be interpolated by an bicubic polynom:

$$z(x,y) = (\mathbf{HY})^T \underbrace{\begin{pmatrix} z(0,0) & z(1,0) & \frac{dz}{dy}(0,0) & \frac{dz}{dy}(1,0) \\ z(0,1) & z(1,1) & \frac{dz}{dy}(0,1) & \frac{dz}{dy}(1,1) \\ \frac{dz}{dy}(0,0) & \frac{dz}{dy}(1,0) & 0 & 0 \\ \frac{dz}{dy}(0,1) & \frac{dz}{dy}(1,1) & 0 & 0 \end{pmatrix}}_{\mathbf{G}} (\mathbf{HY}) \tag{9.1}$$

with

$$\mathbf{X} = \begin{pmatrix} x^3 \\ x^2 \\ x^1 \\ 1 \end{pmatrix} \quad \mathbf{Y} = \begin{pmatrix} y^3 \\ y^2 \\ y^1 \\ 1 \end{pmatrix} \tag{9.2}$$

and

$$\mathbf{H} = \begin{pmatrix} 2 & -3 & 0 & 1 \\ -2 & 3 & 0 & 0 \\ 1 & -2 & 1 & 0 \\ 1 & -1 & 0 & 0 \end{pmatrix} \tag{9.3}$$

The derivatives $\frac{dz}{dx}$ and $\frac{dz}{dy}$ can be found with:

$$\frac{dz}{dx}(x,y) = (\mathbf{HY})^T \mathbf{G}(d\mathbf{HX}) \tag{9.4}$$

$$\frac{dz}{dy}(x,y) = (d\mathbf{HY})^T \mathbf{G}(\mathbf{HX}) \tag{9.5}$$

with

$$d\mathbf{H} = \begin{pmatrix} 0 & 6 & -6 & 0 \\ 0 & -6 & 6 & 0 \\ 0 & 3 & -4 & 1 \\ 0 & 3 & -2 & 0 \end{pmatrix} \tag{9.6}$$

Hence, the normal vector as function of (x,y) is:

$$\mathbf{n}(x,y) = \begin{pmatrix} 1 \\ 0 \\ \frac{dz}{dx}(x,y) \end{pmatrix} \times \begin{pmatrix} 0 \\ 1 \\ \frac{dz}{dy}(x,y) \end{pmatrix} \tag{9.7}$$

The local road plane can now be easily determined:

$$\mathbf{e}_n(x,y) = \frac{n(x,y)}{|n(x,y)|} \tag{9.8}$$

and

$$d(x,y) = \begin{pmatrix} x \\ y \\ z(x,y) \end{pmatrix} \cdot \mathbf{e}_n(x,y); \tag{9.9}$$

9.2 Computation of the contact point

An iterative approximation can be used to find the contact point. A first guess of the contact point's xy-coordinates is made out of the wheel's position. With this information a first estimation of $\mathbf{e}_n(x,y)$ and $d(x,y)$ is possible, which leads to a renewed guess of the contact point position. Again $\mathbf{e}_n(x,y)$ and $d(x,y)$ can be estimated and these mutual estimations could go on forever. If the road surface's curvature is not to strong (as stated above) the series of estimations converges and we can stop the algorithm after a fixed number of iterations.

A straight forward implementation of the solution presented above is only possible for wheel models with tyre. A rigid or an ideal rolling wheel can't be implemented in this fashion. The iterative approximation of the contact point won't lead to a feasible holonomic constraint.

Chapter 10

Summary

The step by step development of models for wheels and tyres has finally led to seven models with an increasing level of complexity:

1. Ideal rolling wheels
2. Rigid wheels with slip
3. Simple slick tyred wheels
4. Simple tread tyred wheels
5. Tread tyred wheels with implicit lat. and long. deformation and a linearized solution
6. Tread tyred wheels with implicit lat. and long. deformation
7. Tread tyred wheels with explicit (contact point shift) lat. and long. deformation

In the WheelDynamics library there is a single model for each level of complexity. In addition a MultiLevel model has been developed to facilitate a switch between these levels. Levels 3-6 can be combined used in combination with uneven road models like sketched in the last chapter.

Appendix A

Notations

The table below covers the notation and meaning of all important variables and parameters. Some of them aren't mentioned in this report, because they were only needed in the implementation. This table should be a valuable assistance to understand the Modelica models in the WheelDynamics library.

The abbreviation r.i.i.f placed behind most of the vectors means: "resolved in inertial frame". All other vectors are resolved in their body (e. g. wheel) frame.

symbol	Modelica	description	type	unit
positional states and their derivatives				
$\mathbf{r}_0$	r_0	position of wheel frame r.i.i.f.	real[3]	m
$\mathbf{v}_0$	v_0	velocity of wheel frame r.i.i.f.	real[3]	m/s
$\mathbf{a}_0$	a_0	acceleration of wheelframe r.i.i.f.	real[3]	m/s2
ω	w	angular vel. of wheel	real[3]	rad/s
ω_0	w_0	angular vel. of wheel r.i.i.f.	real[3]	rad/s
ω_{roll}	w_roll	angular vel. in direction of rolling r.i.i.f.	real[3]	rad/s
ω_{turn}	w_turn	angular vel. in direction of turning r.i.i.f.	real[3]	rad/s
$\mathbf{z}$	z	angular acc. of wheel	real[3]	rad/s2
specification of mass and inertia				
m	m	mass of wheel	real	kg
$\mathbf{I}$	I	inertia tensor of wheel	real[3][3]	kgm2
specification of wheel geometry and road plane				
r	r	outer radius of wheel	Real	m
width	width	width of wheel	Real	m
rCurvature	rCurvature	radius of wheel's curvature	Real	m
$\mathbf{n}_0$	n_0	normal vector of road plane r.i.i.f.	Real[3]	m
d	d	distance of plane to origin	Real	m
additional vectors				
$\mathbf{e}_n$	eN	unit normal vector of road plane r.i.i.f.	Real[3]	1
$\mathbf{e}_{lat}$	eLat	unit vector in road plane in lateral direction r.i.i.f.	Real[3]	1
$\mathbf{e}_{long}$	eLong	unit vector in road plane in longitudinal dir. r.i.i.f.	Real[3]	1
$\mathbf{e}_{wheelAxis}$	eWheelAxis	unit vector parallel to wheel axis r.i.i.f.	Real[3]	1
$\mathbf{p}_{WA}$	pWA	projection of wheel axis on road plane r.i.i.f.	Real[3]	1
contact point and contact region				

symbol	Modelica	description	type	unit
$\mathbf{d}_{CP,0}$	dCP_0	vector from wheel center to contact point r.i.i.f.	Real[3]	m
$\mathbf{r}_{CP,0}$	rCP_0	position of contact point	Real[3]	m
l_{CR}	LCR	length of contact region	Real	m
w_{CR}	WCR	width of contact region	Real	m
l_{trail}	LTrail	length of trail	Real	m
$sign_{trail}$	signTrail	direction of trail	Real	1
$camberDefl$	camberDefl	lateral deflection due to the effect of camber	Real	m
$maxCamberDefl$	maxCamberDefl	maximal possible value for camberDefl	Real	m
slip velocities				
$vSlip$	vSlip	total slip velocity	Real	m/s
$vSlip_{lat}$	vSlipLat	lateral slip velocity	Real	m/s
$vSlip_{long}$	vSlipLong	longitudinal slip velocity	Real	m/s
$vCamberSlip$	vCamberSlip	lateral slip due to camber	Real	m/s
$vRoll$	vRoll	roll velocity	Real	m/s
forces and torques acting on the wheel				
$\mathbf{f}$	f	force acting at wheel center	Real[3]	N
$\mathbf{f}_{tyre,0}$	fTyre	force acting on contact point r.i.i.f.	Real[3]	N
f_n	fN	component of $f_{tyre,0}$ (normal direction)	Real	N
$\hat{f}_n$	fNFric	pseudo normal force relevant to friction	Real	N
f_{lat}	fLat	component of $f_{tyre,0}$ (lateral direction)	Real	N
f_{long}	fLong	component of $f_{tyre,0}$ (longitudinal direction)	Real	N
$\mathbf{t}$	t	torque acting on center	Real[3]	Nm
$\mathbf{t}_{TB}$	tTB	torque due to tyre trail r.i.i.f.	Real[3]	Nm
$\mathbf{t}_{roll}$	tRoll	torque due to roll resistance r.i.i.f.	Real[3]	Nm
$\mathbf{t}_{turn}$	tTurn	torque due to turning friction r.i.i.f.	Real[3]	Nm
specification of general friction characteristics				
$f_{n,1}$	fN1	normal load ($f_n2 = 2f_n1$)	Real	N
$\mu_{max,lat,1}$	muMaxLat1	max. friction coeff. at $f_n = f_{n,1}$(lateral slip)	Real	1
$\mu_{max,long,1}$	muMaxLong1	max. friction coeff. at $f_n = f_{n,1}$(long. slip)	Real	1
$\mu_{min,lat,1}$	muMinLat1	sliding friction coeff. at $f_n = f_{n,1}$(lateral slip)	Real	1
$\mu_{min,long,1}$	muMinLong1	sliding friction coeff. at $f_n = f_{n,1}$(long. slip)	Real	1
$\mu_{max,lat,2}$	muMaxLat2	max. friction coeff. at $f_n = f_{n,2}$(lateral slip)	Real	1
$\mu_{max,long,2}$	muMaxLong2	max. friction coeff. at $f_n = f_{n,2}$(long. slip)	Real	1
$\mu_{min,lat,2}$	muMinLat2	sliding friction coeff. at $f_n = f_{n,2}$(lateral slip)	Real	1
$\mu_{min,long,2}$	muMinLong2	sliding friction coeff. at $f_n = f_{n,2}$(long. slip)	Real	1
$vAdhesion$	vAdhesion	region of adhesion	Real	m/s
$vSlide$	sSlide	minimum velocity of sliding	Real	m/s
$sAdhesion1_{lat}$	sAdhesionLat1	lat. slip at max. force transmis. if $f_n = f_{n,1}$	Real	1
$sAdhesion1_{long}$	sAdhesionLong1	long. slip at max. force transmis. if $f_n = f_{n,1}$	Real	1
$sSlide1_{lat}$	sSlideLat1	lateral slip of sliding friction at $f_n = f_{n,1}$	Real	1
$sSlide1_{long}$	sSlideLong1	longitudinal slip of sliding friction at $f_n = f_{n,1}$	Real	1
$sAdhesion2_{lat}$	sAdhesionLat2	lat. slip at max force transmis. if $f_n = f_{n,2}$	Real	1
$sAdhesion2_{long}$	sAdhesionLong2	long. slip at max. force transmis. if $f_n = f_{n,2}$	Real	1
$sSlide2_{lat}$	sSlideLat2	lat. slip of sliding friction at $f_n = f_{n,2}$	Real	1
$sSlide2_{long}$	sSlideLong2	long. slip of sliding friction at $f_n = f_{n,2}$	Real	1
tol	tol	softness of the softmax function	Real	1
μ_{roll}	muRoll	friction coeff. of roll resistance	Real	1
$\mu_{turn,1}$	muTurn1	friction coeff. of turning resistance at $f_n = f_{n,1}$	Real	1
$\mu_{turn,2}$	muTurn2	friction coeff. of turning resistance at $f_n = f_{n,2}$	Real	1
$gain_{Camber}$	gainCamber	transmission from deflection to camber slip	Real	1/m
$gain_{TB}$	gainTB	gain of turn back influence (tyre trail)	Real	1
dynamic friction characteristics				
$\mu_{max,lat}$	muMaxLat	max. friction coeff. (lateral slip)	Real	1
$\mu_{max,long}$	muMaxLong	max. friction coeff. (longitudinal slip)	Real	1

symbol	Modelica	description	type	unit
$\mu_{min,lat}$	muMinLat	sliding friction coeff. (lateral slip)	Real	1
$\mu_{min,long}$	muMinLong	sliding friction coeff. (longitudinal slip)	Real	1
$sAdhesion_{lat}$	sAdhesionLat	lat. slip of maximum force transmission	Real	1
$sAdhesion_{long}$	sAdhesionLong	long. slip of maximum force transmission	Real	1
$sSlide_{lat}$	sSlideLat	lateral slip of sliding friction	Real	1
$sSlide_{long}$	sSlideLong	longitudinal slip of sliding friction	Real	1
$cosSlip$	cosSlip	cosinus of slip direction angle	Real	1
$sinSlip$	sinSlip	sinus of slip direction angle	Real	1
μ_{max}	muMax	maximum friction coeff. in current direction	Real	1
μ_{min}	muMin	sliding friction coeff. in current direction	Real	1
$sAdhesion$	sAdhesion	slip of maximum force transmission	Real	1
$sSlide$	sSlide	slip of sliding friction	Real	1
vAR	vAR	vAdhesion by current rotation	Real	m/s
vSR	vSR	vSlide by current rotation	Real	m/s
$\dot{\mu}_{vSlip}(0)$	mu0_d	derivative of characterisitc curve at $vSlip = 0$	Real	1
$\frac{d\mu_{vSlip}}{dvSlip}$	muVSlip_d	derivative of characteristic curve	Real	1
$\frac{\mu_{vSlip}}{vSlip}$	muDivVSlip	current frict. coeff. divided by vSlip	Real	s/m
μ_{turn}	muTurn	friction coeff. of turning resistance	Real	1
		spring damping systems		
s_n	sN	travel of virtual tyre spring (normal direction)	Real	m
s_{lat}	sLat	travel of virtual tyre spring (lateral direction)	Real	m
s_{long}	sLong	travel of virtual tyre spring (longitudinal direction)	Real	m
c_n	cN	spring constant(normal direction)	Real	N/m
c_{lat}	cLat	spring constant (lateral direction)	Real	N/m
c_{long}	cLong	spring constant(longitudinal direction)	Real	N/m
d_n	dN	damping constant(normal direction)	Real	Ns/m
d_{lat}	dLat	damping constant (lateral direction)	Real	Ns/m
d_{long}	dLong	damping constant(longitudinal direction)	Real	Ns/m

Bibliography

[1] Georg Rill: **Simulation von Kraftfahrzeugen**. Vieweg, 1994.

[2] Hans B. Pacejka: **Tyre and Vehicle Dynamics**. Butterworth Heinemann, 2002.

[3] G. Aumann, K. Spitzmüller: **Computerorientierte Geometrie**. B.I. Wissenschaftsverlag, 1993.

[4] Martin Otter, Hilding Elmquist and Sven Erik Mattsson: **The New Modelica MultiBody Library**. Proceedings of the 3rd International Modelica Conference, 2003.

[5] H. Elmquist M. Otter, J. Díaz López: **Collision Handling for the Modelica MultiBody Library**. Proceedings of the 4th International Modelica Conference, 2005.

[6] J. Andreasson: **Vehicle Dynamics library**. Proceedings of the 3rd International Modelica Conference, 2003.

[7] David Gordon Wilson: **Bicycling Science**. MIT Press, 2004.

[8] Donald Bastow: **Car Suspension and Handling**. Pentech Press, 1980.

[9] Karl J. Aström, Richard E. Klein, Anders Lennartsson: **Bicycle Dynamics and Control**. To appear in IEEE Control Systems Magazine, August 2005.